IEEE Access
Multidisciplinary | Rapid Review | Open Access Journal

Received February 14, 2020, accepted March 2, 2020, date of publication March 19, 2020, date of current version April 22, 2020.

Digital Object Identifier 10.1109/ACCESS.2020.2982001

A Low-Complexity Equalizer for Video Broadcasting in Cyber-Physical Social Systems Through Handheld Mobile Devices

AHMAD A. A. SOLYMAN[1], HANI ATTAR[2], MOHAMMAD R. KHOSRAVI[3], VARUN G. MENON[4], (Senior Member, IEEE), ALIREZA JOLFAEI[5], (Senior Member, IEEE), VENKI BALASUBRAMANIAN[6], BUVANA SELVARAJ[7], AND POOYA TAVALLALI[8]

[1]Department of Electrical and Electronics Engineering, Istanbul Gelisim University, 34310 Avcılar, Turkey
[2]Department of Energy Engineering, Zarqa University, Zarqa 13134, Jordan
[3]Department of Electrical and Electronic Engineering, Shiraz University of Technology, Shiraz 71555-313, Iran
[4]Department of Computer Science and Engineering, SCMS School of Engineering and Technology, Ernakulam 683576, India
[5]Department of Computing, Macquarie University, Macquarie Park, NSW 2109, Australia
[6]School of Science, Engineering and Information Technology, Federation University, Ballarat, VIC 3350, Australia
[7]School of Information Technology and Engineering, Melbourne Institute of Technology, Melbourne, VIC 3000, Australia
[8]Department of Electrical Engineering and Computer Science, University of California at Merced, Merced, CA 95343, USA

Corresponding authors: Ahmad A. A. Solyman (aaasahmed@gelisim.edu.tr) and Venki Balasubramanian (v.balasubramanian@federation.edu.au)

ABSTRACT In Digital Video Broadcasting-Handheld (DVB-H) devices for cyber-physical social systems, the Discrete Fractional Fourier Transform-Orthogonal Chirp Division Multiplexing (DFrFT-OCDM) has been suggested to enhance the performance over Orthogonal Frequency Division Multiplexing (OFDM) systems under time and frequency-selective fading channels. In this case, the need for equalizers like the Minimum Mean Square Error (MMSE) and Zero-Forcing (ZF) arises, though it is excessively complex due to the need for a matrix inversion, especially for DVB-H extensive symbol lengths. In this work, a low complexity equalizer, Least-Squares Minimal Residual (LSMR) algorithm, is used to solve the matrix inversion iteratively. The paper proposes the LSMR algorithm for linear and nonlinear equalizers with the simulation results, which indicate that the proposed equalizer has significant performance and reduced complexity over the classical MMSE equalizer and other low complexity equalizers, in time and frequency-selective fading channels.

INDEX TERMS Least-squares minimal residual (LSMR), digital video broadcasting-handheld (DVB-H), orthogonal frequency division multiplexing (OFDM), zero-forcing (ZF) and cyber-physical social systems.

I. INTRODUCTION

The Digital Video Broadcasting-Handheld (DVB-H) technology is the superset of the Digital Video Broadcasting-Terrestrial (DVB-T) systems for handheld devices applied in a cyber-physical human organization to share multimedia content. It adopts Orthogonal Frequency Division Multiplexing (OFDM) in its physical layer (as to the OFDM capability to diagonalize the circulant time-invariant channel matrix that allows the use of a single tap equalizer). Indeed, applying a single tap equalizer is considered mandatory for the DVB-H, due to the need for reducing the power consumption to meet the particular requirements of the handheld and battery-powered receivers, taking into consideration that the simplicity feature is achieved only under stationary communication channel conditions. However, in the presence of the carrier frequency offset or Doppler shift (doubly dispersive channel) [1], which is the case in communication channel for DVB-H; the circulant property of the effective channel matrix is no more valid, and therefore the optimality of OFDM against Inter-Carrier Interference (ICI) is lost because the OFDM becomes unable to

The associate editor coordinating the review of this manuscript and approving it for publication was Xiaokang Wang.

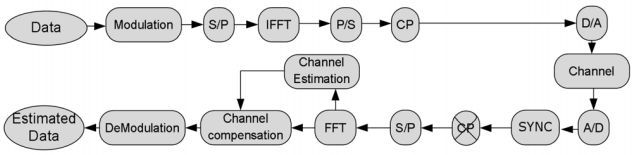

FIGURE 1. OFDM block diagram.

diagonalize the channel matrix anymore. Hence, the need for complex equalizer arises. Replacing the Discrete Fractional Fourier Transform (DFrFT) with the Fast Fourier Transform (FFT) in multicarrier systems reduces the effects of Doppler frequency spreads [2], because the chirped nature of the DFrFT subcarriers mitigates the Doppler shift, and reduces the ICI. However, although DFrFT provides better performance than OFDM under the doubly dispersive fading channel, but yet the complex equalizer is still required [3]. The equalizer complexity is initiated from the need to inverse the channel matrix, which could reach a matrix order up to 8k $*$ 8k in DVB-H typical applications used in Cyber-Physical-Social Systems. Simple equalizers proposed in [4]–[6], rely on iterative methods, or banded matrix inversion to solve the inversion problem. One of the most recent approaches to address the inversion matrix complicatedness is the LSMR algorithm [7], [8], which is an iterative algorithm for sparse least-squares problems that promises better numerical stability, and faster convergence compared to LSQR [9].

In this paper, DFrFT-OCDM and OFDM systems equalization problem will be stated, and a comparison between well-implemented complicated equalizers will be provided. Finally, a novel linear and nonlinear equalization methods will be introduced based on LSMR.

The rest of the paper is organized as follows. Section 2 provides a comprehensive introduction to DFrFT-OCDM and OFDM systems. On the other hand, OFDM and DFrFT-OCDM equalization techniques under doubly dispersive fading channel are introduced in section 3. In section 4, the linear and nonlinear low-complexity LSMR equalizers are explained. Sections 5, illustrates the simulation results with clear justification, and finally, the conclusion is presented in section 6.

II. DFrFT-OCDM AND OFDM SYSTEMS EQUALIZATION

The OFDM block diagram system is shown in Fig. 1 and its received symbols are given by:

$$r_n = HF^* d_n + z_n \tag{1}$$

where r_n is the received sequence, H is the N×N channel matrix that is a linear time-invariant frequency-selective Additive white Gaussian noise channel (AWGN), N is the number of subcarriers, F is the DFT matrix, F* is the Inverse Discrete Fourier Transform (IDFT) matrix, d_n is the transmitted data vector in the n^{th} OFDM symbol, and z_n is the noise in the time domain. After applying the demodulation using a Discrete Fourier Transform (DFT), the received vector becomes:

$$\tilde{r}_n = FHF^* d_n + Fz_n \tag{2}$$

Due to the Cyclic Prefix (CP), H becomes a circulant matrix, and $FHF^{\Lambda *}$ becomes a diagonal matrix [10]. Accordingly, the phase and amplitude of the received sequence can hence be equalized by a simple adjustment.

When the channel is time and frequency selective, or there is a frequency offset in the receiver; the simple equalization procedure fails because the DFT cannot diagonalize the channel matrix any longer, resulting in appearing the ICI; consequently, a complicated equalizer is required that depends on the inversion of the estimated channel matrix [11]–[13], such as an MMSE equalizer. Martone [2] proposed the Fractional Fourier Transform as a new base for the OFDM that can improve the system performance under time and frequency selective fading channel, due to its chirp carrier's nature that can compensate the effect of the Doubler shift [14]. DFrFT-OCDM system will be discussed carefully in the next section.

A. DISCRETE FRACTIONAL FOURIER TRANSFORM (DFrFT)

The FrFT maps a function into an intermediate domain between the time and frequency that may be understood as a rotational operator in the time-frequency plane. The FrFT has an order of α; at which the value of α =0, there will be no changing after applying DFrFT, while for $\alpha = \pi/2$, FrFT becomes a conventional Fourier transform. For other values of α, the DFrFT rotates the time-frequency distribution according to α. The transformation kernel of the continuous FrFT is defined in equation [15], the derivation for [15] is given as follows:

$$K_\alpha(t,u) = A_\alpha e^{j\pi\left(t^2+u^2\right)cot\alpha - j2\pi tucsc\alpha} \tag{3}$$

where α is the rotational angle for the transformation process and

$$A_\alpha = \frac{e^{\{-j\pi\, sign[sin\alpha]/4 + j\alpha/2\}}}{\sqrt{|sin\alpha|}} \tag{4}$$

The forward FrFT is defined as,

$$f_\alpha\{x(t)\}(u) = X_\alpha(u) = \int_{-\infty}^{\infty} x(t) K_\alpha(t,u)\, dt \tag{5}$$

$$x(t) = \int_{-\infty}^{\infty} X_\alpha(u) K_{-\alpha}(t,u)\, du \tag{6}$$

The domains of the signal for $0 < |\alpha| < \pi$ are defining the fractional Fourier domains. Substituting the value of $\alpha = \pi/2$ in (5) and (6) yields the well-known Fourier transform. There are various DFrFT algorithms with different accuracies and properties. Still the DFrFT proposed in [16] is chosen in this proposed work because of its transformation kernel, and its inverse transform is orthogonal and reversible.

Assume that the input function $f(t)$ and the output function $F_\alpha(u)$ of the DFrFT have the chirp period of an order p,

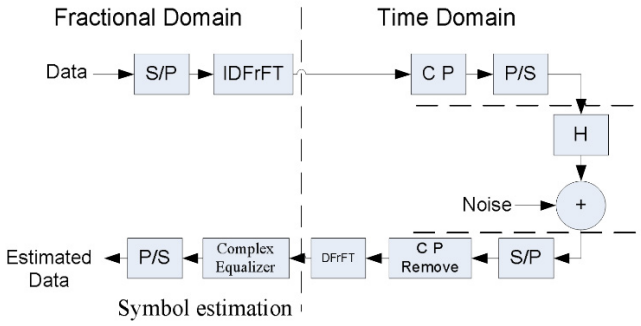

FIGURE 2. The DFrFT-OFDM system with a complicated equalizer.

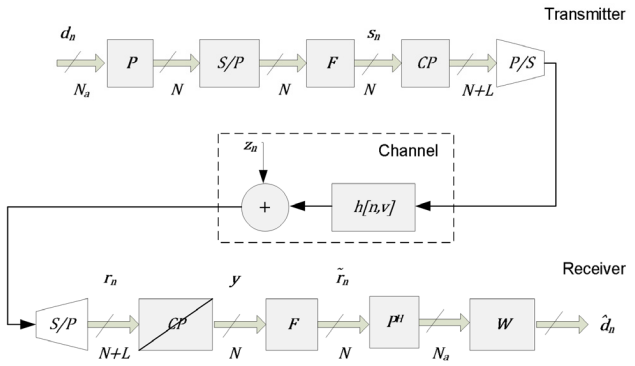

FIGURE 3. The OFDM design.

a period of $T_p = N\Delta t, F_p = M\Delta u$, and sampled signals are with the intervals of Δt and Δu as:

$$x(n) = f(n\Delta t), \quad X_\alpha(m) = F_\alpha(m\Delta u) \tag{7}$$

where n = 0,1... N-1, and m = 0,1... M-1.

When $\alpha \neq D\times\pi$ (D is an integer), (6) can be converted to:

$$X_\alpha(m) = A_\alpha \Delta t e^{\frac{j}{2}cot\alpha.m^2\Delta u^2} \sum_{n=0}^{N-1} \times e^{\frac{j}{2}cot\alpha.n^2\Delta t^2} e^{jcsc\alpha.n.m.\Delta t.\Delta u} x(n) \tag{8}$$

The transformation becomes reversible when M = N, and maintain the condition of (9),

$$\Delta t\Delta u = \frac{2\pi \sin\alpha}{M} \tag{9}$$

Equation (8) can also be written in a matrix-vector multiplication form,

$$X = F_\alpha x \tag{10}$$

where $X = [X\alpha(0), X\alpha(1), .,X\alpha(N-1)]^{\mathrm{T}}$, $x = [x(0), x(1), \ldots, x(N-1)]^{\mathrm{T}}$, and F_α is an $N*N$ matrix. Accordingly, the IDFrFT can be written as:

$$x = F_{-\alpha} X \tag{11}$$

where $F_{-\alpha} = F_\alpha^H$

To remove the Inter-Symbol Interference (ISI), CP is added at the beginning of The DFrFT-OCDM symbol. However, in DVB-H, a larger ICI is introduced. Hence, complicated equalizers are needed, such as in the case of OFDM systems.

The complexity of the DFrFT-OCDM system is almost the same as the OFDM system [2], [8], [17], and both cannot diagonalize the time-variant channel matrix. However, the DFrFT-OCDM can compress the power spreading in the channel matrix much more efficiently than OFDM.

III. OFDM AND DFrFT-OCDM EQUALIZATION TECHNIQUES UNDER DOUBLY DISPERSIVE FADING CHANNEL UNITS

In an OFDM and DFrFT-OCDM systems; the loss of subcarrier orthogonality occurs as a result of the receiver mobility, because the resulted Doppler frequency and time-variation in the frequency fading channel over a Multiple Constant Multiplication (MCM) block period, produces ICI that degrades the OFDM and the DFrFT-OCDM system performance. The ICI increases significantly with the increase of the MCM block size, which is the case in the DVB-H, carrier frequency and velocity. Numerous techniques have been suggested to counter such ICI effects in the OFDM system, and in the DFrFT-OCDM system, such as in [4]–[6], [12], [18]–[23], and [8], [13], [14], respectively.

It has been shown in [11], [18] that nonlinear equalizers based on ICI cancellation generally outperform linear approaches. However, the linear schemes still preserve their importance for the following reasons:

1) Linear equalizers are usually simpler, and therefore less complicated systems are in need of them.
2) Nonlinear schemes usually apply a linear equalizer to obtain the temporary decisions to cancel out the ICI.

Consider the OFDM system in Fig. 3. The transmitted data vector in the n^{th} OFDM symbol is sampled by $d_n = [d_0, d_1 \ldots d_{N_a-1}]^T$ in the frequency domain, and permuted by the binary matrix P that assigns a data vector $d_n \in \mathbb{C}^{N_a}$ to N subcarriers, of which only N_a are active according to:

$$P = \left[0_{N_a\times(N-N_a)/2} I_{N_a} \quad 0_{N_a\times(N-N_a)/2}\right] \tag{12}$$

where $0_{X\times Y}$ is a $X \times Y$ matrix with zero entries, and I_X is a $X \times X$ identity matrix. The vector $s_n = [s_0 s_1 \ldots s_N]^T$ is calculated from:

$$s_n = F^* P d_n \tag{13}$$

where F^* is used to denote to the N-point unitary IDFT matrix.

The doubly dispersive channel can be modelled by the time-variant discrete impulse response $h(n, v)$, where n is the time instant, and v is the time delay. The model justification can be found in more details in [1], [24], [25] and it can be expressed in the form of (time-variant, circular) convolution matrix by:

$$[H]_{n,v} := h(n, \langle n - v\rangle_N) \tag{14}$$

Assuming causal channel and the cyclic prefix L is longer than the maximum delay spread $N_h \leq L$, the received samples

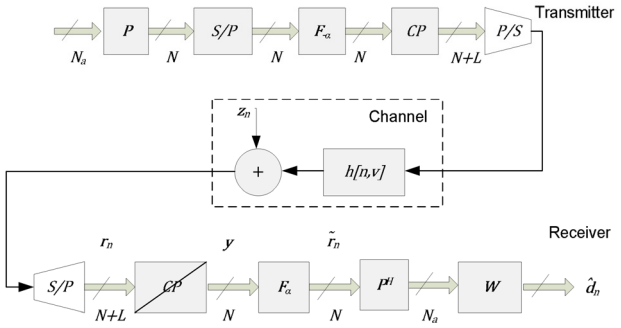

FIGURE 4. DFrFT-OCDM system design.

for the n^{th} OFDM symbol after discarding the CP can be given by:

$$r_n = H_n d_n + z_n \tag{15}$$

where z_n are the samples of AWGN with variance σ^2. In stationary conditions, H_n is circulan and can be decoupled by the DFT matrix. Received subcarriers are demodulated using the DFT

$$y = Fr_n \tag{16}$$

where F is the DFT matrix, and y is the received signal after demodulation by the DFT matrix. The Equalizer matrix $W_n \in \mathbb{C}^{N_a \times N_a}$ operates on the input:

$$\tilde{r}_n = P^H F H_n F^* P d_n + P^H F z = U_n d_n - \tag{17}$$

with a system matrix $U_n \in \mathbb{C}^{N_a \times N_a}$, where $U_n = P^H F H_n F^* P$. The purpose of the binary matrix P is not only to act as a frequency guard band and help lower out-of-band emissions, but also to eliminate components that would appear in the upper right and lower left corners in U_n [4]. The estimated data vector is given by:

$$\hat{d}_n = W \tilde{r}_n \tag{18}$$

where W is the Equalizer matrix, $N_a \times N_a$ is the equivalent subcarrier coupling matrix (frequency domain channel matrix), and the noise vector in the frequency domain are given by $\tilde{H} = FHF^*$; and $\tilde{z} = Fz$, respectively.

It is straight forward to show that $\left[\tilde{H}\right]_{m,k} = \tilde{h}(m-k,k)$, where

$$\tilde{h}(m,k) = \frac{1}{N} \sum_{n=0}^{N-1} \sum_{v=0}^{N-1} h(n,v) e^{-j2\pi(vk+mn)/N} \tag{19}$$

From (19), it can be shown that $\{\tilde{h}(0,:)\}$ appears on the main diagonal of $[\tilde{H}]_{m,k}$, $\{\tilde{h}(-1,:)\}$ on the first super-diagonal, $\{\tilde{h}(1,:)\}$ on the first sub-diagonal and so on, accordingly, $\tilde{h}(m,k)$ can be considered as the frequency-domain response, at subcarrier $k+m$, to a frequency-domain impulse centred at subcarrier k, where m can be understood as the Doppler index, and k is the frequency index. Similarly in $h(n,v)$, n can be interpreted as the time index and v as the lag index. Now consider the DFrFT-OCDM system in Fig. 4, it is almost the same as the OFDM system except for the fact that the modulation and demodulation blocks are replaced by the Inverse Fractional Fourier Transform (IDFrFT) and the Fractional Fourier Transform (DFrFT), respectively. Applying the same procedure over the transmitted and received data transmitter is straight forward, which shows that the Equalizer matrix $W_n \in \mathbb{C}^{N_a \times N_a}$ operates on the input:

$$\tilde{r}_n = P^H F_\alpha H_n F_{-\alpha} P d_n + P^H F_\alpha z = U_{n,\alpha} d_n + \tilde{z}_n \tag{20}$$

where F_α is the DFrFT, $F_{-\alpha}$ is the IDFrFT, α is the fractional angle in the fractional domain, and $U_{n,\alpha}$ is the system matrix with $U_{n,\alpha} \in \mathbb{C}^{N_a \times N_a}$. The equivalent $N_a \times N_a$ channel matrix and the noise vector in the fractional domain are given by $\tilde{H}_\alpha = F_\alpha H F_{-\alpha}$ and $\tilde{z} = F_\alpha z$, respectively.

Both of $\tilde{H}$ and $\tilde{H}_\alpha$ are nondiagonal subcarrier channel matrices resulting of introduce ICI, which is the case when the dispersive channel comprises multipath doubly dispersive channel. Accordingly, the symbol estimation task particularly complicated due to the necessity of a complicated Equalizer.

The linear ZF [26] and MMSE estimates [4] can be found by minimizing $E\{\|d_n - W\tilde{r}_n\|\}$, yielding:

$$\hat{d}_{ZF} = \tilde{H}_\alpha^+ \tilde{r}_n = \tilde{H}_\alpha^H \left(\tilde{H}_\alpha \tilde{H}_\alpha^H\right)^{-1} \tilde{r}_n \tag{21}$$

$$\hat{d}_{MMSE} = \tilde{H}_\alpha^H \left(\tilde{H}_\alpha \tilde{H}_\alpha^H + \gamma^{-1} I_{N_a}\right)^{-1} \tilde{r}_n \tag{22}$$

where $\tilde{H}_\alpha$ can be reduced to $\tilde{H}$ when $\alpha = \pi/2$ and the fractional domain will reduce to the frequency domain, $\hat{d}_{ZF}$ and $\hat{d}_{MMSE}$ are the estimated data after ZF and MMSE equalization, respectively, $\tilde{H}_\alpha^H$ is the channel matrix conjugate transpose in the fractional domain, I_{N_A} is the identity matrix with $N_a \times N_a$ elements, γ is the signal-to-noise ratio (SNR), and $\tilde{H}_\alpha^+$ is the Moore-Penrose pseudo-inverse of the channel matrix in the fractional domain [8], [14], [23]. In (21) and (22), perfect knowledge of the channel matrix H_α is assumed, so the Equalizer does not use guard subcarriers. Furthermore, it is supposed $E\{d_n\} = E\{\tilde{z}_n\} = 0, E\left\{d_n d_n^H\right\} = I, E\left\{d_n \tilde{z}_n^H\right\} = 0, E\left\{\tilde{z}_n \tilde{z}_n^H\right\} = \sigma^2 I$.

Taking into consideration that ZF Equalizer performance is usually regarded as low due to the highly expected noise enhancement. On the other hand, the MMSE Equalizer gives the best performance in all linear Equalizers [18]; however, it is very complicated due to the existence of the channel matrix inversion, which needs $\mathcal{O}(N_a^3)$ complex operations [27], accordingly, ZF is regarded as unpractical for high values of N_a, which is the case DVB-H.

Moreover, it is essential to mention that many Equalizers are proposed for reducing the MMSE Equalizer's complexity [4]–[6], [12], [19], [20], [22]. In [4], a serial MMSE Equalizer is proposed, and in [20] banded Equalizers were offered. All these low complexity Equalizers give almost the same or near performance as block MMSE while reducing the complexity of calculations.

As stated in [4], doubly dispersive channels produce a nearly banded channel matrix in the frequency domain and fractional domain, according to this criteria, more complexity

reduction can be achieved by LDL^H factorization [10], [20] instead of direct matrix inversion. In the following sections, low complexity Equalizers will be examined with DFrFT-OCDM and OFDM based on the LSMR iterative algorithm.

IV. LOW-COMPLEXITY LSMR EQUALIZATION

MMSE Equalizer complexity comes from the matrix inversion in (22), so solving the matrix inversion iteratively is regarded as a smart idea to reduce the MMSE Equalizer's complexity. In [9, [28]–[30], authors use the iterative LSQR algorithm, such as in [31], which has superb performance in solving the channel matrix inversion problem (typically ill-conditioned matrix) by early termination of the iterations at low complexity. The complexity order per iteration is $\mathcal{O}(N_a N_h)$ operations, where N_h is the maximum delay of the channel. Thus, the method is mostly smart when the channel's maximum delay is not too long. Recently, an iterative algorithm called LSMR was proposed in [7].

LSMR is an iterative algorithm for solving linear systems of $Ax = b$, Least-Squares (LS) problems of $min\,\|\text{Ax-b}\|_2$, and Regularized Least Squares (RLS) of $min\left\|\begin{pmatrix} A \\ \lambda I \end{pmatrix} x - \begin{pmatrix} b \\ 0 \end{pmatrix}\right\|_2$ with A being sparse or a fast linear operator [7]. LSMR is based on the Golub-Kahan bi-diagonalization method, and it is analytically equivalent to the MINRES [32], which is applied to the standard equation of $A^T Ax = A^T b$. LSMR is similar in style to the well-known method LSQR in being based on the Golub-Kahan bi-diagonalization of A.

LSQR is equivalent to the Conjugate Gradient (CG) method applied to the standard equation, where $(A^T A + \lambda^2 I)x = A^T b$, which has the property of reducing $\|\boldsymbol{r}_k\|$ monotonically, where $r_k = b - Ax_k$ is the residual for the approximate solution x_k. On the other hand, LSMR has the property of reducing both $\|r_k\|$ and $\|A^T r_k\|$ monotonically. Although LSQR and LSMR ultimately converge to similar points, however, LSMR converges faster at fewer amounts of iterations. LSMR can solve the inversion matrix problem in MMSE Equalizer more effectively with less computational cost due to its higher conversion speed of solution.

A. LSMR ALGORITHM

LSMR algorithm aims to solve the linear equation approximately given by:

$$A^T Ax = A^T b \tag{23}$$

$$min\,\|\text{Ax-b}\|_2 \tag{24}$$

and the regularized least-squares are given by:

$$(A^T A + \lambda^2 I)x = A^T b \tag{25}$$

$$min\left\|\begin{pmatrix} A \\ \lambda \end{pmatrix} x - \begin{pmatrix} b \\ 0 \end{pmatrix}\right\|_2 \tag{26}$$

where A is being sparse or a fast linear operator.

The flow chart for the LSMR algorithm is shown in Fig. 5.

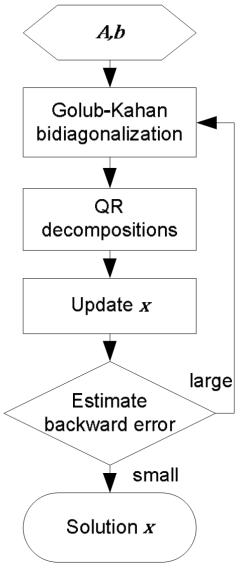

FIGURE 5. LSMR algorithm flow chart.

For simplicity, consider (23) given $A(m \times n)$ and $b(m \times 1)$ starting from Golub-Kahan bi-diagonalization [33], the direct bi-diagonalization is provided by:

$$U^T (b\ A) \begin{pmatrix} 1 & \\ & V \end{pmatrix} = \begin{pmatrix} \times & \times & 0 & 0 \\ 0 & \times & \times & 0 \\ 0 & 0 & \times & \times \\ 0 & 0 & 0 & \times \end{pmatrix}$$

$$\Rightarrow (bAV) = U\,(\beta_1 e_1 B) \tag{27}$$

using iterative bi-diagonalization Bidiag (A, b):

$$b = U_{k+1}\,(\beta_1 e_1) \tag{28}$$

$$AV_k = U_{k+1} B_k \tag{29}$$

$$A^T U_k = V_k B_k^T \begin{pmatrix} I_k \\ 0 \end{pmatrix} \tag{30}$$

where

$$B_k = \begin{pmatrix} \alpha_1 & 0 & 0 & 0 \\ \beta_1 & \alpha_2 & 0 & 0 \\ 0 & \ddots & \ddots & 0 \\ 0 & 0 & \beta_k & \alpha_k \\ 0 & 0 & 0 & \beta_{k+1} \end{pmatrix} \tag{31}$$

and

$$U_k = \begin{pmatrix} u_1 & \ldots & u_k \end{pmatrix}$$
$$V_k = \begin{pmatrix} v_1 & \ldots & v_k \end{pmatrix}$$

V_k spans the Krylov subspace:

$$\text{span}\left\{ v_1, \ldots, v_k \right\} = \text{span}\left\{ A^T b, \left(A^T A\right) A^T b, \ldots, \left(A^T A\right)^{k-1} A^T b \right\} \tag{32}$$

Define $x_k = V_k y_k$, sub-problem to solve:

$$\min_{yk} \left\|A^T r_k\right\| = \min_{yk} \left\| \bar{\beta}_1 e_1 - \begin{pmatrix} B_k^T B_k \\ \bar{\beta}_{k+1} e_k^T \end{pmatrix} \right\| \tag{33}$$

where $r_k = b - Ax_k$, $\bar{\beta}_k = \alpha_k \beta_k$

TABLE 1. Storage and computational requirements for various *LS* methods.

	Storage		Work	
	m	n	m	n
LSMR	$\boldsymbol{Av}, \boldsymbol{u}$	$\boldsymbol{x}, \boldsymbol{v}, \boldsymbol{h}, \bar{\boldsymbol{h}}$	3	6
LSQR	$\boldsymbol{Av}, \boldsymbol{u}$	$\boldsymbol{x}, \boldsymbol{v}, \boldsymbol{w}$	3	5
MINRES On $\boldsymbol{A^TAx = A^Tb}$	$\boldsymbol{Av}$	$\boldsymbol{x}, \boldsymbol{v_1}, \boldsymbol{v_2}, \boldsymbol{w_1}, \boldsymbol{w_2}, \boldsymbol{w_3}$	-	8

B. LSMR COMPLEXITY

The storage requirement and computational complexity can be compared for LSMR and LSQR on $Ax \approx b$, and MINRES on the normal equation $A^TAx = A^Tb$. The vector storage (excluding the storage of A and b) was listed in Table 1. Taking into consideration that A is $(m \times n)$ for LS systems, where m might be considerably larger than n. Moreover, Av denotes to the working storage for the matrix-vector products, h_k and; $\bar{h}_k$ are scalar multiples of $w_k, \bar{w}_k$, respectively, and the work represents the number of floating-point multiplications required for each iteration.

From Table 1, it can be shown that the complexity of the LSMR is slightly more than the LSQR.

C. LINEAR LSMR EQUALIZERS

1) LINEAR LEAST SQUARES LSMR EQUALIZER

The doubly dispersive channel matrix is characterized by large maximum delay and Doppler shifts. So the system matrix (Fractional domain channel matrix) $\tilde{H}_\alpha$ might have a very high condition number, and the linear least squares (LLS)-LSMR can be used for equalization with ''implicit regularization.''

Using the LLS-LSMR equaliser directly on $\tilde{\boldsymbol{H}}_\alpha$ will be complex. However, applying LLS-LSMR on $\boldsymbol{B}_n$ produces a major complexity drop, taking into consideration that the banded properties of $\tilde{\boldsymbol{H}}_\alpha$ and using $\boldsymbol{B}_n = \boldsymbol{M} \odot \tilde{H}_\alpha$ where $\odot$ represents element-wise multiplication, and

$$\boldsymbol{M}\,(m, n) = \begin{cases} 1 & 0 \le |\text{m-n}| \le Q \\ 0 & Q < |\text{m-n}| < N_a \end{cases}$$

Accordingly, the typical equation for LLS-LSMR Equalizer is then given by:

$$B_n^H B_n \hat{d}_{ZF} = B_n^H \tilde{r}_n \tag{34}$$

This standard equation is obtained from (20) when ignoring the noise $\tilde{z}_n$, substituting $\tilde{H}_\alpha$ with B_n, and left-multiplying by B_n^H. One can show that in the i^{th} LSMR iteration, an approximate solution for the linear least squares problem is obtained by $min \left\| B_n \hat{d}_{ZF} - \tilde{r}_n \right\|$.

In zero-forcing equalizer, ignoring the noise effect results in noise and modelling errors amplification that degrades the system's performance. The same can be considered for LLS-LSMR Equalizer, because there is no account for noise effect. However, LSMR depends on the number of iterations as a regularization parameter, accordingly; an efficient way of avoiding the amplification of errors and noise can be ensured by early termination of the amount of the iterations. Consequently, using the optimal number of iterations in LSMR can reduce the system's errors to a comparable limit with the MMSE equalisation. In practice, LSMR inputs are known approximately, and using the maximum number of iteration amplifies the noise and modelling errors.

2) REGULARIZED LEAST SQUARES LSMR EQUALIZER

The estimated data $\tilde{d}_{MMSE}$ from (30) in the MMSE sense is given by:

$$\hat{d}_{MMSE} = \tilde{H}_\alpha^H \left(\tilde{H}_\alpha \tilde{H}_\alpha^H + \gamma^{-1} I_{N_a} \right)^{-1} \tilde{r}_n \tag{35}$$

which is equivalent to:

$$\hat{d}_{MMSE} = \left(\tilde{H}_\alpha^H \tilde{H}_\alpha + \gamma^{-1} I_{N_a} \right)^{-1} \tilde{H}_\alpha^H \tilde{r}_n \tag{36}$$

by multiplying the left side of (36) by $\left(\tilde{H}_\alpha^H \tilde{H}_\alpha + \gamma^{-1} I_{N_a} \right)$; (37) is obtained:

$$\left(\tilde{H}_\alpha^H \tilde{H}_\alpha + \gamma^{-1} I_{Na} \right) \hat{d}_{MMSE} = \tilde{H}_\alpha^H \tilde{r}_n \tag{37}$$

which is equivalent to the regularized least-squares problem $(A^TA + \lambda^2 I)x = A^Tb$ to minimize $min \left\| \begin{pmatrix} A \\ \lambda \end{pmatrix} x - \begin{pmatrix} b \\ 0 \end{pmatrix} \right\|_2$ RLS-LSMR Equalizer.

Again, the obtained system is complex when working for the entire $\tilde{H}_\alpha$ matrix, which justifies using the banded properties of $\tilde{H}_\alpha$ that leads to the banded matrix B_n, the MMSE Equalizer problem applying the band approximation will be given by:

$$\left(B_n B_n^H + \gamma^{-1} I_{N_a} \right) \hat{d}_{MMSE} = B_n^H \tilde{r}_n \tag{38}$$

It is can be shown that an approximate solution of the regularized least-squares equation can be reached using the LSMR.

In this method, RLS-LSMR has two regularization parameters: the number of iterations and the signal to noise ratio (γ) parameter, which limits the noise and modelling errors amplification, and improves the system performance.

The optimal number of LSMR iterations depends on:

1) The noise level.
2) The maximum Doppler spread and the maximum delay spread as they affect the distribution of the singular values of the channel matrix.

However, the number of iterations does not depend on the number of subcarriers, which appears clearly in simulation.

LSMR is particularly attractive due to its numerical stability, inherent potential for regularization, and low computational complexity of $\mathcal{O}(N_a(Q+1)i)$ complex operations in total [7], where i denotes to the number of iterations used, N_a number of subcarriers, and Q is the number of sub - and super-diagonals that define the banded matrix limits.

Thus, the complexity is just linear in N_a, Q, and the number of iterations i.

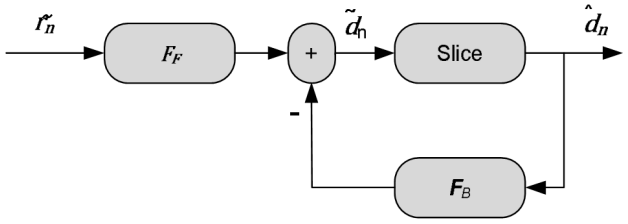

FIGURE 6. BDFE structure.

D. NONLINEAR LSMR EQUALIZERS

1) LOW COMPLEXITY LSMR-BASED BLOCK DECISION FEEDBACK EQUALIZER (LSMR-BDFE) FOR DFrFT-OCDM)

The Block decision feedback Equalizer (BDFE) was proposed in [34] to improve the MMSE Equalizer performance by detecting the data recursively (one-by-one) instead of detecting all of them concurrently. Hence, the consecutive detection technique was used, which is extensively adopted in DS-CDMA systems for multi-user detection.

An Equalizer based on the LSMR and the MMSE-BDFE was designed to reduce the MMSE-BDFE Equalizer complexity and to improve the performance. Unlike the previously mentioned techniques; the proposed Equalizer uses the LSMR algorithm to minimize the band approximation error, and uses the band LDL^H factorization method with DFE to obtain better performance without increasing the complexity. The MMSE methodology in [34] was adopted to design the feed-forwarded (F_F), and feedback (F_B) filters as shown in Fig. 6. This methodology minimizes the error $e = \tilde{d}_n - d_n$. Considering that F_B is strictly the upper triangular, resulting to enable the feed-back process to be performed by successive cancellation.

Using the standard assumption of correct past decisions, that is $\tilde{\boldsymbol{d}}_n = \boldsymbol{d}_n$; the error vector can be expressed as below.

$$e = F_F \tilde{r}_n - \left(F_B + I_{N_a}\right) d_n \tag{39}$$

which leads to the relation between F_F and F_B according to the mean square error (MSE) minimization criterion in [34]:

$$\begin{aligned} F_F &= (F_B + I_{Na}) \left(\tilde{H}_\alpha^H \tilde{H}_\alpha + \gamma^{-1} I_{Na}\right)^{-1} \tilde{H}_\alpha^H \\ &= (F_B + I_{Na})\, W_{MMSE} \end{aligned} \tag{40}$$

by applying the band approximation $\tilde{H}_\alpha = B_n$

$$F_F = (F_B + I_{Na}) \left(B_n B_n^H + \gamma^{-1} I_{Na}\right)^{-1} B_n^H \tag{41}$$

The feed-forwarded filter is the cascade of the low-complexity MMSE Equalizer and an upper triangular matrix $F_B + I_{Na}$ with unit diagonal. Designing the feed-forwarded and the feed-back filters were carried out in details in [34], where the autocorrelation matrix of the error vector e is given by:

$$R_{ee} = \sigma^2 \left(F_B + I_{N_a}\right) \left(B_n B_n^H + \gamma^{-1} I_{N_a}\right)^{-1} \left(F_B + I_{N_a}\right)^H \tag{42}$$

where σ^2 is the noise variance. Using the LDL^H:

$$M = B_n B_n^H + \gamma^{-1} I_{Na} = LDL^H \tag{43}$$

where L is the lower triangular with unit diagonal, and D is the diagonal matrix. It is straight forward now to minimize the error expectation $E\left\{\boldsymbol{e}^2\right\}$ by setting:

$$F_B = L^H - I_{Na} \tag{44}$$

which reduces R_{ee} diagonal. Using (41) and (44); F_F can be expressed by:

$$F_F = L^H W_{MMSE} = L^H M^{-1} B_n^H = D^{-1} L^{-1} B_n^H \tag{45}$$

Although (45) and (44) looks complicated but using the LSMR algorithm with the fact that D is diagonal, B is banded, and L is lower triangular and banded; it turns out that the resulting banded LSMR-BDFE is then characterized by very low complexity. For the feed-forwarded filter:

$$d_n = F_F \tilde{r}_n \tag{46}$$

$$\tilde{r}_n = F_F^{-1} d_n = B^{-H} DL d_n \tag{47}$$

from (43) it can be shown that:

$$DL = \left(B_n B_n^H + \gamma^{-1} I_{N_a}\right) L^{-H} \tag{48}$$

$$\begin{aligned} \tilde{r}_n &= B_n^{-H} \left(B_n B_n^H + \gamma^{-1} I_{Na}\right) L^{-H} d_n \\ &= \left(B_n + B_n^{-H} \gamma^{-1}\right) L^{-H} d_n \end{aligned} \tag{49}$$

which can be solved efficiently using the LSMR algorithm.

The complexity of the proposed LSMR-BDFE Equalizer is almost the same as the RLS-LSMR Equalizer with a total of $\mathcal{O}(N(Q+1)i)$ complex operations.

E. RLS-LSMR SLIDING WINDOW EQUALIZER

Sliding window Equalizer was proposed in [35] to reduce the complexity of the MMSE Equalizer by dividing the large matrix inversion to a multiple of smaller matrix inversions, for example, the complexity of inverting $N \times N$ matric equal $\mathcal{O}\left(N^3\right)$. So, choosing $N = 96$ gives a complexity equal 884736 complex operations. In comparison, if the inversion was sub-divided to calculate the 96 symbols using a window of 9 so the total complexity will equal $9^3 \times 96 = 69984$, which is less complicated.

Accordingly, the main idea to estimate transmitting a symbol on a particular subcarrier is to consider a small window from the entire banded system matrix B_n, in which all the energy corresponding to the symbol of interest is concentrated in this window while ignoring the rest. This method is then repeated by sliding the window over all the subcarriers of the received multicarrier symbol. Using this technique reduces the dimension of the system under consideration, resulting in reducing the complexity considerably, without decreasing the system's performance significantly.

Based on above, the complexity can be reduced more by merely using the LSMR algorithm in solving the reduced dimension system.

Consider the case where the data symbol $d_{k,n}$ has to be detected; almost all the $d_{k,n}$ symbol energy is located on the subcarrier k and its neighbours. $d_{k,n}$ can be estimated using:

$$\hat{d}_{k,n} = W_{MMSE,k}\tilde{r}_k \tag{50}$$

where the vector $\tilde{r}_k = \left[\tilde{r}_{k-D}\cdots\tilde{r}_{k+D}\right]^T$ is a part of the received vector $\tilde{r}$, which is related to the symbol $d_{k,n}$ and its neighbours, $P = 2D + 1$ is the number of the related symbols that equal to the size of the sliding window matrix $(P \times K)$, $K = (2Q + 1)$, Q is the number of sub- and super-diagonals that defines the banded matrix limits, and $W_{MMSE,k}$ is the MMSE Equalizer for the k symbol window:

$$W_{MMSE,k} = \left(B_{n,k}B_{n,k}^H + \gamma^{-1}I_k\right)^{-1}B_{n,k}^H \tag{51}$$

where $B_{n,k}$ matrix is a part of the equivalent banded system matrix B_n with $P \times K$ size and can be defined by:

$$B_{n,k} = \begin{bmatrix} B_{k-D,k-Q} & B_{k-D,k-Q+1} & \cdots & B_{k-D,k+Q} \\ B_{k-D+1,k-Q} & B_{k-D+1,k-Q+1} & \cdots & B_{k-D+1,k+Q} \\ \vdots & \vdots & \vdots & \vdots \\ B_{k+D,k-Q} & B_{k+D,k-Q+1} & \cdots & B_{k-D,k+Q} \end{bmatrix} \tag{52}$$

Using this approach turns the complexity of inverting the $N_a \times N_a$ matrix into N inversions of $P \times K$ matrices, which could be reduced even more by using the LSMR algorithm to solve the regularized least-squares problem:

$$\left(B_{n,k}B_{n,k}^H + \gamma^{-1}I_k\right)\hat{d}_k = B_{n,k}^H\tilde{r}_k \tag{53}$$

Reduction in the system's complexity depends on the width of the sliding window matrix P, taking into consideration that choosing a minimal P does not affect the system's performance significantly. Another hidden benefit from this algorithm is the reduction of the effort for perfect channel matrix estimation, as it is no longer needed because only a limited number of the channel elements are required. The complexity of the sliding window equalizer is given by $\mathcal{O}(N_aP(Q + 1)i_{P\times K})$. Though the first glance may show that the obtained complexity exceeds the complexity of the other LSMR low complexity Equalizers, however, the number of iterations $i_{P\times K}$ needed to solve the smaller matrix $P \times K$ is much fewer than the number of iterations i needed to solve the matrix $N_a \times N_a$, which means that the complexity is reduced in reality.

V. SIMULATION RESULTS

The non-encoded BER performance of the DFrFT-OCDM and the OFDM system with the different LSMR Equalizers are investigated by means of simulation over 10^5 multicarrier blocks. DFrFT-OCDM and OFDM systems with $N = 128$, $N_A = 96$, $L = 8$, and QPSK modulation are assumed. Simulations are performed over an ensemble of 10^5 Rayleigh fading channels defined by an exponential power delay profile with an RMS delay spread of three sampling periods. The channel

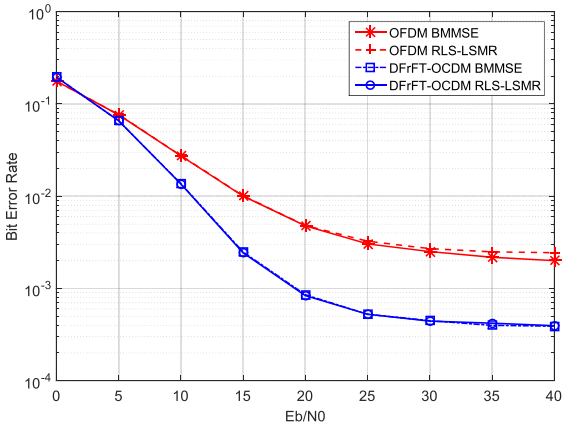

FIGURE 7. DFrFT-OCDM and DFT-OFDM non-coded BER comparison (Q=5).

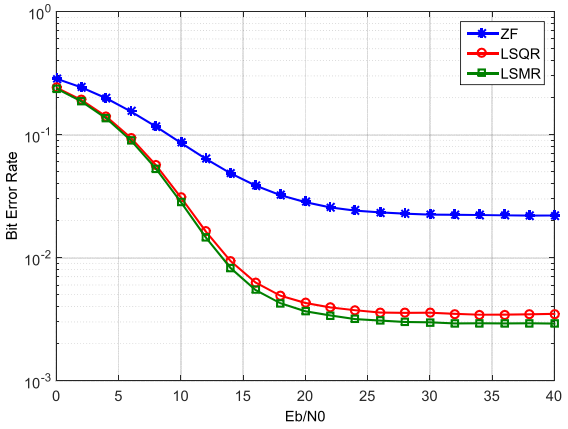

FIGURE 8. Non-coded BER comparison between LSMR, LSQR, and ZF.

model uses the same statistics as in [20], including a maximum Doppler spread f_d equal to 15% of the carrier spacing. The carrier frequency is $f_C = 10$ GHz, and the subcarrier spacing is $\Delta f = 20$kHz. This Doppler frequency corresponds to a high mobile speed $V = 324$ Km/h.

1) LINEAR LSMR EQUALIZER SIMULATION RESULTS

Fig. 7 shows a comparison between the DFrFT-OCDM and the OFDM using $=$ 5, Banded MMSE (BMMSE), and RLS-LSMR Equalizers. From this figure, it can be seen that the DFrFT-OCDM outperforms the OFDM system with both the LSMR and the MMSE Equalizers, though the complexity of the DFrFT-OCDM system is almost the same as the OFDM system.

Fig. 8 compares the performance of the DFrFT-OCDM system using different Equalizers (ZF, LSMR, and LSQR), taking into consideration that LSMR and LSQR algorithms will solve the linear system $Ax = b$ with the limited number of iterations. Fig. 8, illustrates that the LSMR Equalizer provides the best performance and the LSQR Equalizer almost achieves the same performance in low SNR and slightly less than LSMR in higher SNR, which is justified

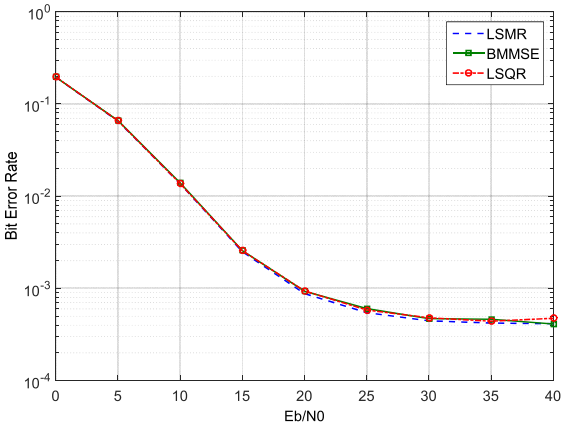

FIGURE 9. Non-coded BER comparison between BMMSE, LSQR and LSMR equalizers.

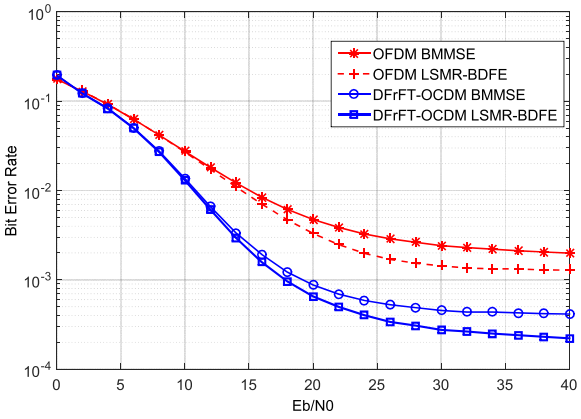

FIGURE 10. DFrFT-OCDM and DFT-OFDM non-encoded BER comparison (Q=5).

by the reason that the LSMR algorithm is more stable than LSQR algorithm. However, the processing with sparse, possibly ill-conditioned least-squares problems, also the LSMR converges faster with a low amount of iterations. On the other hand, the ZF Equalizer provides the worst performance due to the matrix inversion of the sparse matrix B as it amplifies noise. LSMR and LSQR Equalizers reach almost the same performance, with much less complexity than the ZF Equalizer. LSQR can provide the same performance as LSMR using a higher number of iterations, which leads to more complexity.

Fig. 9 shows a comparison between the performance of the DFrFT-OCDM using different Equalizers (LSMR, LSQR, and BMMSE) where LSMR and LSQR will solve the regularized least-squares problem (38). From here, it is clear that all Equalizers give almost the same performance, but the complexity of the LSMR and LSQR Equalizers is much less than the complexity of the MMSE. Moreover, comparing the LSMR and the LSQR shows that both algorithms converge to nearly the same point (though LSMR is better than LSQR). However, the LSMR converges faster at fewer numbers of iterations.

From the numerical simulations shown in Fig. 8 and Fig. 9, it is clear that the minimum achievable BERs for the LLS-LSMR (34) and the RLS-LSMR (38) are close to each other even if the noise limits are identified precisely at the receiver.

However, a key advantage of RLS-LSMR is that the semi-convergence is many minors; that the BER grows gradually as the number of iterations increases after reaching the minimum.

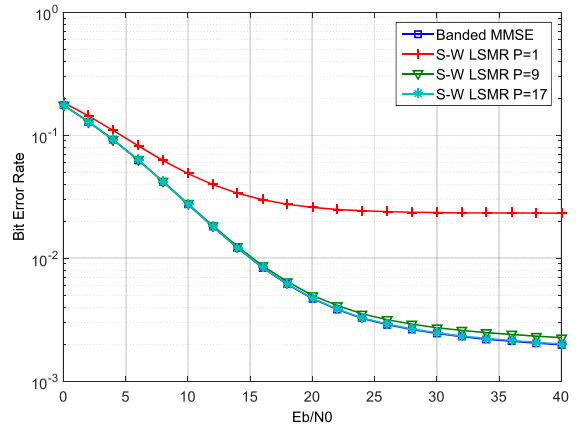

FIGURE 11. RLS-LSMR sliding window equalizer and the banded MMSE equalizer BER comparison (Q=5).

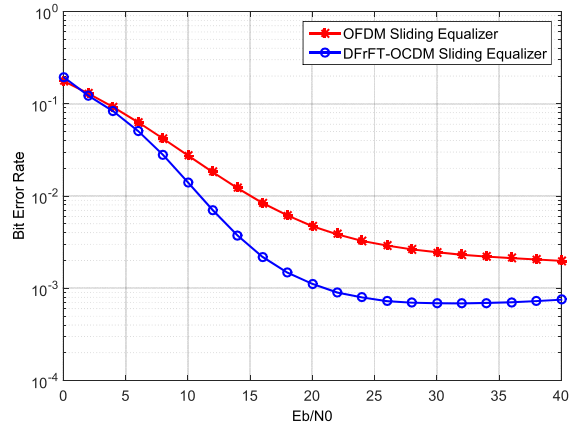

FIGURE 12. DFrFT-OCDM and OFDM non-coded BER comparison using the RLS-LSMR sliding window equalizer.

2) NONLINEAR LSMR EQUALIZER SIMULATION RESULTS

Fig. 10 shows a comparison between the DFrFT-OCDM and the OFDM using $Q = 5$, LSMR-BDFE, and BMMSE Equalizers. It can be perceived from Fig. 10 that the LSMR-BDFE Equalizer provides the best performance, and the BMMSE Equalizer almost give the same performance in low SNR. Again according to Fig. 10, the DFrFT-OCDM outperforms the OFDM system with both the BMMSE and the LSMR-BDFE Equalizers, though the complexity of the DFrFT-OCDM system is almost the same as the OFDM system.

Fig. 11 also provides a comparison between the proposed RLS-LSMR sliding window Equalizer and the banded MMSE Equalizer at $Q = 5$, it can be demonstrated that the banded MMSE Equalizer achieves the best performance and the RLS-LSMR sliding window Equalizer almost provides the same performance in low SNR. Moreover, in high signal to noise ratio, the performance of the RLS-LSMR sliding window Equalizer is slightly degraded, which is the penalty that is paid for reducing the complexity, taking into consideration that the performance degradation depends on the window matrix dimension.

Fig. 12 describes a comparison between the DFrFT-OCDM and the OFDM systems using the proposed RLS-LSMR sliding window Equalizer with $Q = 5$ and $P = 9$. The results illustrate that the DFrFT-OCDM significantly outperforms the OFDM system, which enhances this paper's achievement.

VI. CONCLUSION

In this paper, the doubly dispersive channel and its effect on DVB-H based on OFDM system's performance were investigated towards the social internet of things and cyber-physical human system applications [36]–[43]. DFrFT-OCDM MCM system was investigated as an alternative MCM system that can improve the overall DVB-H system's performance. Low complexity Equalizers were proposed with OFDM and DFrFT-OCDM systems. The results show that using simple Equalizers with DFrFT-OCDM achieves better performance than using the same low complexity Equalizers with OFDM, accordingly, this paper suggest that the offered DFrFT-OCDM system with the LSMR can be used for reliable DVB-H communication. Low complexity Equalizers were offered using the new LSMR algorithm, which provides the same performance though the more moderate complexity when compared to the LSQR and the LDL^{H} factorization algorithms. Using low complexity equalizer while improving or maintain the DVB-H system's performance will increase the hand-held system battery usage time and over-all system reliability. Future is planned to improve the proposed system by applying it to other techniques address complexity, or the power efficiency, such as Network Coding introduced in [44]–[47], or utilizing the proposed equalizer over the optimum number of paths for the realization of multi-path routing in [48].

REFERENCES

[1] T. Wang, J. G. Proakis, E. Masry, and J. R. Zeidler, "Performance degradation of OFDM systems due to Doppler spreading," *IEEE Trans. Wireless Commun.*, vol. 5, no. 6, pp. 1422–1432, Jun. 2006.

[2] M. Martone, "A multicarrier system based on the fractional Fourier transform for time-frequency-selective channels," *IEEE Trans. Commun.*, vol. 49, no. 6, pp. 1011–1020, Jun. 2001.

[3] J. Armstrong, "Analysis of new and existing methods of reducing intercarrier interference due to carrier frequency offset in OFDM," *IEEE Trans. Commun.*, vol. 47, no. 3, pp. 365–369, Mar. 1999.

[4] P. Schniter, "Low-complexity equalization of OFDM in doubly selective channels," *IEEE Trans. Signal Process.*, vol. 52, no. 4, pp. 1002–1011, Apr. 2004.

[5] S. Ahmed, M. Sellathurai, and J. A. Chambers, "Low complexity iterative method of equalization for OFDM in doubly selective channels," in *Proc. 29th Asilomar Conf. Signals, Syst. Comput.*, 2005, pp. 687–691.

[6] L. Rugini, P. Banelli, and G. Leus, "Simple equalization of time-varying channels for OFDM," *IEEE Commun. Lett.*, vol. 9, no. 7, pp. 619–621, Jul. 2005.

[7] D. C.-L. Fong and M. Saunders, "LSMR: An iterative algorithm for sparse least-squares problems," *SIAM J. Sci. Comput.*, vol. 33, no. 5, pp. 2950–2971, Jan. 2011.

[8] A. A. A. Solyman, S. Weiss, and J. J. Soraghan, "Low-complexity LSMR equalisation of FrFT-based multicarrier systems in doubly dispersive channels," in *Proc. IEEE Int. Symp. Signal Process. Inf. Technol. (ISSPIT)*, Dec. 2011, pp. 461–465.

[9] G. Taubock, M. Hampejs, G. Matz, F. Hlawatsch, and K. Grochenig, "LSQR-based ICI equalization for multicarrier communications in strongly dispersive and highly mobile environments," in *Proc. IEEE 8th Workshop Signal Process. Adv. Wireless Commun.*, Jun. 2007, pp. 1–5.

[10] G. H. Golub and C. F. Van Loan, *Matrix Computations*, 3rd ed. Baltimore, MD, USA: Johns Hopkins Univ., 1996.

[11] W. Gi Jeon, K. Hi Chang, and Y. Soo Cho, "An equalization technique for orthogonal frequency-division multiplexing systems in time-variant multipath channels," *IEEE Trans. Commun.*, vol. 47, no. 1, pp. 27–32, Jan. 1999.

[12] L. Rugini and P. Banelli, "Performance analysis of banded equalizers for OFDM systems in time-varying channels," in *Proc. IEEE 8th Workshop Signal Process. Adv. Wireless Commun.*, Jun. 2007, pp. 1–5.

[13] R. Bomfin, D. Zhang, M. Matthe, and G. Fettweis, "A theoretical framework for optimizing multicarrier systems under time and/or frequency-selective channels," *IEEE Commun. Lett.*, vol. 22, no. 11, pp. 2394–2397, Nov. 2018.

[14] M. Nassiri and G. Baghersalimi, "Comparative performance assessment between FFT-based and FRFT-based MIMO-OFDM systems in underwater acoustic communications," *IET Commun.*, vol. 12, no. 6, pp. 719–726, Apr. 2018.

[15] C. Candan, M. A. Kutay, and H. M. Ozaktas, "The discrete fractional Fourier transform," *IEEE Trans. Signal Process.*, vol. 48, no. 5, pp. 1329–1337, May 2000.

[16] H. M. Ozaktas, O. Arikan, M. A. Kutay, and G. Bozdagt, "Digital computation of the fractional Fourier transform," *IEEE Trans. Signal Process.*, vol. 44, no. 9, pp. 2141–2150, Sep. 1996.

[17] M. N. Hussin, "FrFT-based EO-STBC multicarrier system for transmission over doubly-dispersive channels," in *Proc. Int. Symp. Wireless Commun. Syst. (ISWCS)*, 2012, pp. 686–690.

[18] Y.-S. Choi, P. J. Voltz, and F. A. Cassara, "On channel estimation and detection for multicarrier signals in fast and selective Rayleigh fading channels," *IEEE Trans. Commun.*, vol. 49, no. 8, pp. 1375–1387, Aug. 2001.

[19] T. Hrycak and G. Matz, "Low-complexity time-domain ICI equalization for OFDM communications over rapidly varying channels," in *Proc. Fortieth Asilomar Conf. Signals, Syst. Comput.*, 2006, pp. 1767–1771.

[20] L. Rugini, P. Banelli, and G. Leus, "Low-complexity banded equalizers for OFDM systems in Doppler spread channels," *EURASIP J. Adv. Signal Process.*, vol. 2006, no. 1, Dec. 2006, Art. no. 67404.

[21] R. Kumar and S. Malarvizhi, "Time-domain equalization technique for intercarrier interference suppression in OFDM systems," in *Proc. 15th Int. Conf. Adv. Comput. Commun.*, Dec. 2007, pp. 391–396.

[22] H. Doğan, E. Panayirci, and H. V. Poor, "Low-complexity joint data detection and channel equalisation for highly mobile orthogonal frequency division multiplexing systems," *IET Commun.*, vol. 4, no. 8, pp. 1000–1011, 2010.

[23] F. Rottenberg, X. Mestre, F. Horlin, and J. Louveaux, "Efficient equalization of time-varying channels in MIMO OFDM systems," *IEEE Trans. Signal Process.*, vol. 67, no. 21, pp. 5583–5595, Nov. 2019.

[24] X. Cai and G. B. Giannakis, "Bounding performance and suppressing intercarrier interference in wireless mobile OFDM," *IEEE Trans. Commun.*, vol. 51, no. 12, pp. 2047–2056, Dec. 2003.

[25] Y. Li and L. J. Cimini, "Bounds on the interchannel interference of OFDM in time-varying impairments," *IEEE Trans. Commun.*, vol. 49, no. 3, pp. 401–404, Mar. 2001.

[26] K. Chen-Hu and A. G. Armada, "Low-complexity computation of zero-forcing equalizers for massive MIMO-OFDM," in *Proc. IEEE 89th Veh. Technol. Conf. (VTC-Spring)*, Apr. 2019, pp. 1–5.

[27] G. H. Golub and C. F. Van Loan, *Matrix Computations*. Baltimore, MD, USA: Johns Hopkins Univ. Press, 1996.

[28] T. Hrycak, S. Das, G. Matz, and H. G. Feichtinger, "Low complexity equalization for doubly selective channels modeled by a basis expansion," *IEEE Trans. Signal Process.*, vol. 58, no. 11, pp. 5706–5719, Nov. 2010.
[29] H. Han and L.-N. Wu, "Low complexity LSQR-based block decision feedback equalizer for OFDM systems over rapidly time-varying channels," in *Proc. Int. Conf. Commun. Mobile Comput.*, Apr. 2010, pp. 438–441.
[30] G. Taubock, M. Hampejs, P. Svac, G. Matz, F. Hlawatsch, and K. Grochenig, "Low-complexity ICI/ISI equalization in doubly dispersive multicarrier systems using a decision-feedback LSQR algorithm," *IEEE Trans. Signal Process.*, vol. 59, no. 5, pp. 2432–2436, May 2011.
[31] C. C. Paige and M. A. Saunders, "LSQR: An algorithm for sparse linear equations and sparse least squares," *ACM Trans. Math. Softw.*, vol. 8, no. 1, pp. 43–71, Mar. 1982.
[32] C. C. Paige and M. A. Saunders, "Solution of sparse indefinite systems of linear equations," *SIAM J. Numer. Anal.*, vol. 12, no. 4, pp. 617–629, Sep. 1975.
[33] G. Golub and W. Kahan, "Calculating the singular values and pseudo-inverse of a matrix," *J. Soc. Ind. Appl. Math. B, Numer. Anal.*, vol. 2, no. 2, pp. 205–224, Jan. 1965.
[34] A. Stamoulis, G. B. Giannakis, and A. Scaglione, "Block FIR decision-feedback equalizers for filterbank precoded transmissions with blind channel estimation capabilities," *IEEE Trans. Commun.*, vol. 49, no. 1, pp. 69–83, Jan. 2001.
[35] I. Ivan and B. Muquet, "Reduced complexity decision feedback equalizer for supporting high mobility in wimax," in *Proc. IEEE 69th Veh. Technol. Conf.*, Apr. 2009, pp. 1–5.
[36] X. Wang, L. T. Yang, X. Xie, J. Jin, and M. J. Deen, "A cloud-edge computing framework for Cyber-Physical-Social services," *IEEE Commun. Mag.*, vol. 55, no. 11, pp. 80–85, Nov. 2017.
[37] X. Wang, W. Wang, L. T. Yang, S. Liao, D. Yin, and M. J. Deen, "A distributed HOSVD method with its incremental computation for big data in Cyber-Physical-Social systems," *IEEE Trans. Comput. Social Syst.*, vol. 5, no. 2, pp. 481–492, Jun. 2018.
[38] X. Wang, L. T. Yang, H. Li, M. Lin, J. Han, and B. O. Apduhan, "NQA: A nested anti-collision algorithm for RFID systems," *ACM Trans. Embedded Comput. Syst.*, vol. 18, no. 4, pp. 1–21, Jul. 2019, doi: 10.1145/3330139.
[39] X. Wang, L. T. Yang, Y. Wang, X. Liu, Q. Zhang, and M. J. Deen, "A distributed tensor-train decomposition method for cyber-physical-social services," *ACM Trans. Cyber-Phys. Syst.*, vol. 3, no. 4, pp. 1–15, Oct. 2019, doi: 10.1145/3323926.
[40] L. Qi, X. Zhang, S. Li, S. Wan, Y. Wen, and W. Gong, "Spatial-temporal data-driven service recommendation with privacy-preservation," *Inf. Sci.*, vol. 515, pp. 91–102, Apr. 2020.
[41] S. Wan and S. Goudos, "Faster R-CNN for multi-class fruit detection using a robotic vision system," *Comput. Netw.*, vol. 168, Feb. 2020, Art. no. 107036.
[42] L. Qi, W. Dou, W. Wang, G. Li, H. Yu, and S. Wan, "Dynamic mobile crowdsourcing selection for electricity load forecasting," *IEEE Access*, vol. 6, pp. 46926–46937, 2018.
[43] S. Wan, Z. Gu, and Q. Ni, "Cognitive computing and wireless communications on the edge for healthcare service robots," *Comput. Commun.*, vol. 149, pp. 99–106, Jan. 2020.
[44] H. Attar, L. Stankovic, and V. Stankovic, "Cooperative network-coding system for wireless sensor networks," *IET Commun.*, vol. 6, no. 3, pp. 344–352, 2012.
[45] S. Nazir, V. Stankovic, H. Attar, L. Stankovic, and S. Cheng, "Relay-assisted rateless layered multiple description video delivery," *IEEE J. Sel. Areas Commun.*, vol. 31, no. 8, pp. 1629–1637, Aug. 2013.
[46] H. Attar, L. Stankovic, M. Alhihi, and A. Ameen, "Deterministic network coding over long term evaluation advance communication system," in *Proc. 4th Int. Conf. Digit. Inf. Commun. Technol. Appl. (DICTAP)*, May 2014, pp. 56–61.
[47] M. El-Hihi, H. Attar, A. A. A. Solyman, and L. Stankovic, "Network coding cooperation performance analysis in wireless network over a lossy channel, M users and a destination scenario," *Commun. Netw.*, vol. 8, pp. 257–280, 2016, doi: 10.4236/cn.2016.84023.
[48] M. A. Alhihi, M. R. Khosravi, H. Attar, and M. Samour, "Determining the optimum number of paths for realization of multi-path routing in MPLS-TE networks," *TELKOMNIKA Indonesian J. Electr. Eng.*, vol. 15, no. 4, pp. 1701–1709, 2017.

AHMAD A. A. SOLYMAN received the degree from the University of Strathclyde, U.K., in 2013. His Ph.D. researches include in multimedia services over wireless networks using OFDM. He is currently a Lecturer with the Department of Electrical and Electronics Engineering, Istanbul Gelisim University, Turkey. His research interests contain wireless communication networks and MIMO communication systems.

HANI ATTAR received the Ph.D. degree from the Department of Electrical and Electronic Engineering, University of Strathclyde, U.K., in 2011. Since 2011, he has been working as a Researcher of electrical engineering and energy systems. He is currently a University Lecturer with Zarqa University, Jordan. His research interests include network coding, wireless sensor networks, and wireless communications.

MOHAMMAD R. KHOSRAVI received the B.Sc., M.Sc., and Ph.D. degrees electrical engineering with expertise in communications and signal processing. He has been with Department of Electrical and Electronic Engineering, Shiraz University of Technology, Shiraz, Iran. He is currently with the Department of Computer Engineering, Persian Gulf University, Bushehr, Iran. His main interests include statistical signal and image processing, medical bioinformatics, radar imaging and satellite remote sensing, computer communications, industrial wireless sensor networks, underwater acoustic communications, information science, and scientometrics.

VARUN G. MENON (Senior Member, IEEE) is currently an Associate Professor with the Department of Computer Science and Engineering, SCMS School of Engineering and Technology, India. He has published more than 50 research articles in peer reviewed and highly indexed international journals and conferences. His research interests include the Internet of Things, fog computing and networking, underwater acoustic sensor networks, scientometrics, educational psychology, ad-hoc networks, wireless communication, opportunistic routing, and wireless sensor networks. He has served more than 20 conferences like IEEE ICC, ICCCN 2020, IEEE COINS 2020, SigTelCom, ICACCI, and ICDMAI in leadership capacities including a Program Co-Chair, a Track Chair, a Session Chair, and a Technical Program Committee Member. He is currently a Guest Editor of the IEEE TRANSACTIONS ON INDUSTRIAL INFORMATICS, the IEEE SENSORS JOURNAL, the *IEEE Internet of Things Magazine*, and the *Journal of Supercomputing*. He is an Associate Editor of *IET Quantum Communications* and also an Editorial Board Member of the IEEE FUTURE DIRECTIONS. He is a Distinguished Speaker of ACM.

ALIREZA JOLFAEI (Senior Member, IEEE) received the Ph.D. degree in applied cryptography from Griffith University, Gold Coast, Australia. He worked as an Assistant Professor with Federation University Australia and Temple University, Philadelphia, USA. He is currently a Lecturer (Assistant Professor in North America) and a Program Leader of cyber security with Macquarie University, Sydney, Australia. He has authored more than 60 peer-reviewed articles on topics related to cybersecurity. His current research areas include cyber security, the IoT security, human-in-the-loop CPS security, cryptography, AI, and machine learning for cyber security. He has received multiple awards for Academic Excellence, University Contribution, and Inclusion and Diversity Support. He received the prestigious IEEE Australian council award for his research article published in the IEEE TRANSACTIONS ON INFORMATION FORENSICS AND SECURITY.

VENKI BALASUBRAMANIAN received the Ph.D. degree in body area wireless sensor network (BAWSN) for remote healthcare monitoring applications. He is the pioneer in building (pilot) remote healthcare monitoring application (rHMA) for pregnant women for the New South Wales Healthcare Department. His research established a dependability measure to evaluate rHMA that uses BAWSN. His research also opened up a new research area in measuring time-critical applications. He contributed immensely to eResearch software research and development that uses cloud-based infrastructure and a software architect for the several projects sponsored by Australian National Data Service (ANDS). He contributed heavily in the field of healthcare informatics, sensor networks, and cloud computing. He is the Founder of Anidra Tech Ventures Pty Ltd., a smart remote patient monitoring company.

BUVANA SELVARAJ received the master's degree in software science from Periyar University, India. She is currently an Academician with the School of Information Technology and Engineering, Melbourne Institute of Technology, Australia. Her research interests are in android programming, software engineering, and the IoT.

POOYA TAVALLALI received the B.Sc. and M.Sc. degrees in electrical engineering (communication systems) from the Department of Electrical and Electronic Engineering, Shiraz University, Shiraz, Iran, in 2013 and 2016, respectively. He is currently pursuing the Ph.D. degree with the Department of Electrical Engineering and Computer Science, University of California at Merced, Merced, USA. His scientific interest consists of machine learning, statistical signal and image processing, neural networks, statistical pattern recognition, and optimization algorithms.